Spin-polarized electron capture for the $Na+{}^3He^{2+}$ system at a ${}^3He^{2+}$ impact energy of 5.33–9.33 keV/amu

M. Tanaka
Kobe Tokiwa Jr. College, Ohtani-cho 2-6-2, Nagata, Kobe 653, Japan

N. Shimakura
Department of Chemistry, Niigata University, Igarashinino-machi 8050, Niigata 950-21, Japan

T. Ohshima
The Spring-8 Project Team, Kamigori-cho, Hyogo 678-12, Japan

K. Katori
Laboratory of Nuclear Studies, Osaka University, Machikaneyama-cho 1-1, Toyonaka, Osaka 565, Japan

M. Fujiwara, H. Ogata, and M. Kondo
Research Center for Nuclear Physics, Osaka University, Mihogaoka 10-1, Ibaraki, Osaka 567, Japan
(Received 5 January 1994)

${}^3He^+$ atomic polarizations following the spin-polarized electron capture process for the $\vec{Na}(3s)+{}^3He^{2+}$ system were measured at ${}^3He^{2+}$ impact energies from 5.33 to 9.33 keV/amu. The magnitude of the ${}^3He^+$ atomic polarizations was deduced from the ${}^3He^+$ nuclear polarization measured by means of beam-foil spectroscopy. The observed polarization transfer coefficient P_T defined by the ratio of the ${}^3He^+$ atomic polarization to the sodium one showed a pronounced reduction from unity, which was qualitatively explained by the prediction of a simple cascade photon decay model. Evidence for a further reduction of P_T from the above model and a possible impact energy dependence of P_T suggested an excessive depolarization due to the presence of the collision alignment parameter $A_0^{\rm col}$ of ${}^3He^+$ formed by the electron capture process. In order to see this more closely, the observed P_T's were examined theoretically using the semiclassical impact parameter method, in which an 18-state molecular expansion was employed, and atomic-type electron translation effects were rigorously taken into account. Ensuring that both the absolute values and the impact energy dependence of the observed capture cross sections were remarkably well reproduced by the calculations in which the states up to $4f$ in ${}^3He^+$ were introduced, it was demonstrated that the calculated results for P_T qualitatively reproduced not only the absolute values of the observed P_T's but also their gentle decrease with increasing impact energy. Production of nuclear polarizations resulting from the polarized electron capture processes between multicharged heavy ions and alkaline-earth-metal atoms is offered as one of the promising applications to the future project of universal polarized heavy-ion sources.

PACS number(s): 34.70.+e, 34.80.Nz, 03.65.Sq, 34.10.+x

I. INTRODUCTION

Electron-capture processes in ion-atom collisions have often been of practical importance as well as fundamental interest in understanding atomic collision mechanisms. In the thermonuclear fusion problem these processes are crucial, since they make plasma temperatures lower due to energy-loss collisions having negative Q values. Further attention to the importance of the capture processes in alkaline atoms is also paid because it is useful in diagnostics for properties of the hot plasma [1]. Alternately, as a possible means of obtaining an ultrahigh vacuum or soft-x-ray laser beam, specific electron-capture processes with lithium enabling a population inversion between the ground and excited states of the projectile was suggested by Vinogradov and Sobelman [2].

Investigation of the electron-capture processes has so far been carried out mainly through total cross-section measurements on a variety of combinations of atoms and ions over a broad impact energy range. For a detailed understanding of mechanisms active in collision processes, however, the increasingly sophisticated measurements are indispensable along with spin-polarization and correlation effects. Such spin studies have initially been on either electron-atom or atom-atom collision processes in order to investigate, for instance, the collision mechanism for spin-polarized electrons tracing the behavior of individual electrons or effects upon the trajectory [3] and the rotational couplings [4] with a collision-induced alignment of the final state. In contrast, owing to technical difficulties in producing and manipulating polarized atoms and ions, the electron-capture processes in ion-

atom collisions with spin-polarized partners have long been beyond our reach even though the theory analogous to the electron-atom system might be valid.

Meanwhile, a novel idea for polarizing a proton beam using the electron-capture processes between an incident proton and a polarized alkaline atom was proposed [5,6] more than a decade ago and later employed as a practical polarized ion source [7] dedicated to nuclear physics research. The above idea recently succeeded in polarizing such heavier nuclei as ^3He [8] and ^{14}N [9]. Since the primary aim of the above capture processes has been restricted to practical use in polarized ion sources, theoretical investigation of the detailed collision mechanisms has not been attempted in spite of its physical importance.

In the present paper we report on the polarization measurement and the theoretical understanding of the electron-capture processes for the $\vec{Na}(3s)+{}^3He^{2+}$ system in an impact $^3He^{2+}$ energy range of 5.33–9.33 keV/amu. The need to develop a polarized ^3He ion source [8] employing this spin-polarized electron-capture process has motivated this study. The achievable $^3He^+$ nuclear polarization is dependent upon impact energy like the capture process itself. Therefore, one should search for the $^3He^{2+}$ impact energy at which $^3He^+$ nuclear polarization is maximized. The limit upon the impact energy range covered in the present work, i.e., 5.33–9.33 keV/amu, was due to experimental constraints.

As mentioned in Sec. IV, a sizable reduction of the $^3He^+$ polarization relative to the initial sodium polarization was found. Most of this reduction is not caused by the capture process itself but the polarization losses during cascade photon emissions of $^3He^+$ (cascade photon decay model). However, reduction of the $^3He^+$ polarization beyond that predicted by the simple cascade photon decay model exists. This suggests additional depolarization processes during the photon emissions. This additional reduction may be due to the collision alignment parameter $A_0^{\rm col}$ generated by the capture process.

Calculations attempting to reproduce the observed polarization transfer coefficients defined by the ratios of the $^3He^+$ atomic to the initial sodium polarizations were carried out using a semiclassical impact-parameter method, which has proven validity at the present impact energy range. The present collision system allows a stringent test of various models because of the simplicity of the collision mechanism. First, collision systems involving alkaline atoms are reliably treated since they effectively represent quasi, one-electron targets due to the relatively loose binding of their single outermost electron. Secondly, the impact particle, i.e., $^3He^{2+}$, has no surrounding electrons. Preliminary data and analysis of our work were presented in Ref. [10].

II. POLARIZATION FOLLOWING PHOTON EMISSIONS

This section describes the cascade photon decay model, in which the $^3He^+$ polarization following cascade photon emissions can be expressed in terms of the initial sodium atomic polarization. A possible scenario for the overall capture process including subsequent cascade photon emissions follows.

In the beginning, a polarized electron of a sodium atom ($3s$) is captured by an incident $^3He^{2+}$ ion to form an excited $^3He^+$ ion with almost no polarization reduction due to a weak spin-orbit interaction [11]. The excited $^3He^+$ state thereafter cascades down to the ground state or the metastable states by emitting photons. During photon emission some of the initial electronic polarization is lost. This indicates that the amount of depolarization depends simply on the photon decay schemes. We thus calculate the final $^3He^+$ polarization following the electron-capture process.

Suppose the electron capture and subsequent photon emissions take place under an external magnetic field sufficiently weak so as not to decouple the LS coupling but strong enough to decouple the hyperfine coupling, the so-called Paschen-Back region. According to a simple formula valid for a hydrogenlike atom expressed by n,J,L, the decoupling field $B_{\rm hf}$ needed to decouple the hyperfine interactions is given by

$$B_{\rm hf} \geq \frac{\mu_0}{4\pi}\frac{4g_I\mu_e\mu_N}{g_I\mu_N - g_J\mu_e}\frac{1}{J(J+1)(2L+1)}\frac{Z^3}{a_\mu^3 n^3}\ , \quad (1)$$

where μ_0 is the magnetic permeability in the vacuum, a_μ is the reduced radius of a hydrogenlike atom, g_I is the nuclear g factor, and μ_e and μ_N are the Bohr and nuclear magneton, respectively. For the ground $1s$ state of the $^3He^+$ ion, $B_{\rm hf}$ is estimated to be 0.31 T. Fortunately, this condition is almost realized in our system where the magnetic field of 0.3 T is applied to the region of the capture process as described in Sec. IV. On the other hand, the magnetic field necessary for the LS decoupling is estimated to be more than 30 T by simply scaling the well established proton case [12], assuming that the necessary decoupling field is proportional to $Z^4/\{n^3 l(l+1)\}$ [13], where Z is the atomic number of the incident ion and n and l are a principal and orbital quantum number of the capture electron orbit, respectively.

With the external magnetic field of 0.3 T, we will perform the cascade photon decay model proposed by Liu and Dunford [14]. Assuming the quantization axis is parallel to the beam propagation direction, the state multipole ${}^J\rho_q^k$ of $^3He^+$ formed by the electron capture is given by

$${}^I\rho_q^k = \sum_{k_L,k_S,q_L,q_S} [(2k_L+1)(2k_S+1)(2J+1)(2J+1)]^{1/2} \begin{Bmatrix} L & S & J \\ L & S & J \\ k_L & k_S & k \end{Bmatrix} (-)^{k-q}\sqrt{2k+1} \begin{pmatrix} k_L & k & k_S \\ q_L & -q & q_S \end{pmatrix} {}^L\rho_{q_L}^{k_L}(0)\,{}^S\rho_{q_S}^{k_S}(0)\ , \quad (2)$$

where ${}^{L}\rho(0)^{k_L}_{q_L}$ and ${}^{S}\rho(0)^{k_S}_{q_S}$ are the orbital and spin part of the state multipoles, and k, k_L, and k_S are the rank of each state multipole, respectively. Since relevant photon transitions are all electric dipole ($E1$) and the $E1$ operator acts only on L, the state multipole ${}^{J_i}\rho^k_q$ for the J_i state after photon emission is simply expressed in terms of the state multipole ${}^{J_{i+1}}\rho^k_q$ for the J_{i+1} state as

$$ {}^{J_i}\rho^k_q = C_i B(k,J_i,J_{i+1})\,{}^{J_{i+1}}\rho^k_q \ , \tag{3} $$

where C_i and $B(k,J_i,J_{i+1})$ are respectively given by

$$ C_i = |\langle C_i' < L_{i+1}\|\mathbf{r}\|L_i > |^2 \ , \tag{4} $$

$$ B(k,J_i,J_{i+1}) = (2J_{i+1}+1)(2J_i+1)(-)^{J_{i+1}+J_i+1+k} \times \begin{Bmatrix} L_{i+1} & J_{i+1} & S \\ J_i & L_i & 1 \end{Bmatrix}^2 \begin{Bmatrix} J_{i+1} & J_i & 1 \\ J_i & J_{i+1} & k \end{Bmatrix} , \tag{5} $$

where C' is a constant. Assuming that the final J_0 state is populated in combination with various cascade transitions denoted by $J_N \to J_{N-1} \to \cdots \to J_0$, the final-state multipole ${}^{J_0}\rho^k_q$ is, therefore, described by using Eqs. (3) and (4),

$$ {}^{J_0}\rho^k_q = \prod_i C_i \sum_{J_N} D(k,J_0,J_N)\,{}^{J_N}\rho^k_q \ , \tag{6} $$

where $D(k,J_0,J_N)$ is given by

$$ D(k,J_0,J_N) = \sum_{J_1,J_2,\ldots,J_{N-1}} B(k,J_0,J_1)B(k,J_1,J_2)\cdots \times B(k,J_{N-1},J_N) \ . \tag{7} $$

Equation (6) indicates that the state multipole for the final $1s$ ground state ($J_0=\frac{1}{2}$) following the cascade photon emissions can be connected to the initial-state multipole with J_N.

The initial-state multipole in Eq. (6) is, on the other side, expressed in terms of the product of the orbital state multipole with L and the spin multipole with $S=\frac{1}{2}$, as described in Eq. (2). In this case, the initial-state multipoles with $q\neq 0$ vanish because of the symmetry around the polarization direction, which coincides with the beam propagation direction. Since we are concerned only with vector polarization, i.e., a rank $k=1$, the polarization of the ground state is defined by

$$ P_e(1s) = \frac{{}^{S}\rho^1_0}{{}^{S}\rho^0_0} \ , \tag{8} $$

and this definition is rewritten in terms of ${}^{J}\rho^1_0$ and ${}^{J}\rho^0_0$ by using Eq. (2) in which $L=0$ is substituted,

$$ P_e(1s) = \frac{{}^{J}\rho^1_0}{{}^{J}\rho^0_0} \ . \tag{9} $$

Substituting Eq. (6) in Eq. (9),

$$ P_e(1s) = \frac{\sum_{J_N} D(1,1/2,J_N)\,{}^{J_N}\rho^1_0(0)}{\sum_{J_N} D(0,1/2,J_N)\,{}^{J_N}\rho^0_0(0)} \ , \tag{10} $$

where ${}^{J_N}\rho^1_0(0)$ and ${}^{J_N}\rho^0_0(0)$ symbolize the state multipoles corresponding to the initial state before photon emissions with ranks of 1 and 0, respectively. Substituting explicit expressions for the state multipoles described by Eq. (2) in the right side of Eq. (10), the polarization $P_e(1s)$ for the final states after photon emission is expressed in terms of the initial-state multipoles. Thus, the denominator of Eq. (10) is

$$ \mathcal{D} = \left[\sum_{J_N} \left\{ \frac{2J_N+1}{(2L+1)(2S+1)} \right\}^{1/2} D(0,\tfrac{1}{2},J_N) \right] \times {}^{L}\rho^0_0(0)\,{}^{S}\rho^0_0(0) \ , $$

and the numerator of Eq. (10) is

$$ \mathcal{N} = -\sum_{J_N}(2J_N+1)D(1,\tfrac{1}{2},J_N) \sum_{k_L,k_S} \sqrt{3(2k_L+1)(2k_S+1)} \begin{Bmatrix} L & S & J_N \\ L & S & J_N \\ k_L & k_S & 1 \end{Bmatrix} \begin{pmatrix} k_L & 1 & k_S \\ 0 & 0 & 0 \end{pmatrix} {}^{L}\rho_0^{k_L}(0)\,{}^{S}\rho_0^{k_S}(0) $$

$$ = -\left[\sum_{J_N}(2J_N+1)D(1,\tfrac{1}{2},J_N)\sqrt{3} \begin{Bmatrix} L & S & J_N \\ L & S & J_N \\ 0 & 0 & 0 \end{Bmatrix} \right] {}^{L}\rho^0_0(0)\,{}^{S}\rho^1_0(0) $$

$$ -\left[\sum_{J_N}(2J_N+1)D(1,\tfrac{1}{2},J_N)\sqrt{6} \begin{Bmatrix} L & S & J_N \\ L & S & J_N \\ 2 & 1 & 1 \end{Bmatrix} \right] {}^{L}\rho_0^{k_L}(0)\,{}^{S}\rho_0^{k_S}(0) \ . $$

Here, the well known properties of the Clebsch-Gordan coefficient and the $9j$ symbol are used. Equation (10) is consequently given by

$$P_e(1s)=A_1\frac{{}^S\rho_0^1(0)}{{}^S\rho_0^0(0)}+A_2\frac{{}^L\rho_0^2(0)}{{}^L\rho_0^0(0)}\frac{{}^S\rho_0^1(0)}{{}^S\rho_0^0(0)}\ , \tag{11}$$

where A_1 and A_2 are respectively given by

$$A_1=-\frac{\sqrt{3}(2L+1)(2S+1)\sum_{J_N}D(1,\frac{1}{2},J_N)\begin{Bmatrix}L&S&J_N\\L&S&J_N\\0&0&1\end{Bmatrix}}{\sum_{J_N}\sqrt{2J_N+1}D(0,\frac{1}{2},J_N)}\ ,$$

$$A_2=-\frac{\sqrt{6}(2L+1)(2S+1)\sum_{J_N}D(1,\frac{1}{2},J_N)\begin{Bmatrix}L&S&J_N\\L&S&J_N\\2&1&1\end{Bmatrix}}{\sum_{J_N}\sqrt{2J_N+1}D(0,\frac{1}{2},J_N)}\ .$$

The term having ${}^S\rho_0^1(0)/{}^S\rho_0^0(0)$ in Eq. (11) corresponds to the initial polarization as shown by

$$P_e(0)=\frac{{}^S\rho_0^1(0)}{{}^S\rho_0^0(0)}\ , \tag{12}$$

and the term having ${}^L\rho_0^2(0)/{}^L\rho_0^0(0)$ in Eq. (11) corresponds to the initial alignment. The alignment is prescribed in terms of the collision alignment parameter $A_0^{\rm col}$ defined by Fano and Macek [15] as

$$\frac{{}^L\rho_0^2(0)}{{}^L\rho_0^0(0)}=\left[\frac{5L(L+1)}{(2L+3)(2L-1)}\right]^{1/2}A_0^{\rm col}\ , \tag{13}$$

where $A_0^{\rm col}$ is represented in terms of the capture cross sections σ_m to the magnetic substate m as

$$A_0^{\rm col}=\frac{\sum_{m=-L}^{L}[3m^2-L(L+1)]\sigma_m}{L(L+1)\sum_{m=-L}^{L}\sigma_m}\ . \tag{14}$$

By substituting Eqs. (12) and (13) in Eq. (11), the ground-state polarization $P_e(1s)$ is expressed in terms of $P_e(0)$ and $A_0^{\rm col}$,

$$P_e(1s)=A_1P_e(0)+A_2\left[\frac{5L(L+1)}{(2L+3)(2L-1)}\right]^{1/2}A_0^{\rm col}P_e(0)\ . \tag{15}$$

It is reasonable to assume that the initial electron polarization $P_e(0)$ is equal to the sodium polarization $P_{\rm Na}$ since the spin-orbit interaction has a minor role in the collision dynamics [11]. Therefore, we can write

$$P_e(0)=P_{\rm Na}\ . \tag{16}$$

The polarization transfer coefficient P_T defined by the ratio of $P_e(1s)$ to $P_{\rm Na}$ is

$$P_T=\frac{P_e(1s)}{P_{\rm Na}}=A_1+A_2\left[\frac{5L(L+1)}{(2L+3)(2L-1)}\right]^{1/2}A_0^{\rm col}\ . \tag{17}$$

Equation (17) indicates that P_T is determined only from the coupling scheme of the angular momenta and the collision alignment parameter $A_0^{\rm col}$ formed by the capture process as long as no depolarization mechanism other than that caused by photon emissions is present. On the other hand, $A_0^{\rm col}$ is determined by the collision dynamics, which indicates that P_T should depend on the impact energy.

Finally, we will numerically evaluate P_T by using Eq. (17) individually for possible cascade photon decay routes. According to the previous analysis [16] of the experimental data [1] for the $^4He^{2+}+Na\rightarrow{}^4He^+ + Na^+$ capture process at incident energies covering our present case it is demonstrated that the transitions to the $n=3$ states, in particular, to the $3d$ and $3p$ states in $^4He^+$, are predominantly populated. Recently, the partial capture cross sections were measured from observation of photons [28]. The result supported the predominance of the $n=3$ capture. As discussed in Sec. V, these aspects were ensured in our present theoretical calculation. Hence we took only the cascade photon decay processes starting from the $3d$, $3p$, $3s$ states in $^3He^+$ into account.

In case of the capture to the $3d$ state in $^3He^+$, three of the cascade routes are possible as classified by

(i) $J_N=\frac{5}{2}$ $(n=3, L=2; 0)\rightarrow J_1=\frac{3}{2}$ $(n=2, L=1)$ $\rightarrow J_0=\frac{1}{2}$ $(n=1, L=0; 1s)$,

(ii) $J_N=\frac{3}{2}$ $(n=3, L=2; 0)\rightarrow J_1=\frac{3}{2}$ $(n=2, L=1)$ $\rightarrow J_0=\frac{1}{2}$ $(n=1, L=0; 1s)$,

(iii) $J_N=\frac{3}{2}$ $(n=3, L=2; 0)\rightarrow J_1=\frac{1}{2}$ $(n=2, L=1)$ $\rightarrow J_0=\frac{1}{2}$ $(n=1, L=0; 1s)$.

In the capture to the $3p$ state in $^3He^+$, possible cascade photon routes become somewhat complex because part of them passes through the $2s$ metastable state in $^3He^+$. However, for simplicity, we consider only two cascade routes denoted by

(iv) $J_N=\frac{3}{2}$ $(n=3, L=1; 0)\rightarrow J_0=\frac{1}{2}$ $(n=1, L=0; 1s)$,

(v) $J_N=\frac{1}{2}$ $(n=3, L=1; 0)\rightarrow J_0=\frac{1}{2}$ $(n=1, L=0; 1s)$.

Even though the capture to the $3s$ state in $^3He^+$ has a small cross section, we took it into account in the present work. Possible cascade photon routes starting from this state are

(vi) $J_N=\frac{1}{2}$ $(n=3, L=0; 0)\rightarrow J_1=\frac{3}{2}$ $(n=2, L=1)$ $\rightarrow J_0=\frac{1}{2}$ $(n=1, L=0; 1s)$,

(vii) $J_N=\frac{1}{2}$ $(n=3, L=0; 0)\rightarrow J_1=\frac{1}{2}$ $(n=2, L=1)$ $\rightarrow J_0=\frac{1}{2}$ $(n=1, L=0; 1s)$.

By using Eq. (17) we can numerically evaluate the polarization transfer coefficients expressed in terms of the initial alignment parameters as summarized below. Concerning the routes starting from the $3d$ state in $^3He^+$ [(i)–(iii)], $P_T(1)$ is expressed by

$$P_T(1)=0.301+0.201A_0^{\rm col}\ , \tag{18}$$

where $A_0^{\rm col}$ for $L=2$ varies from -1 to 1. Concerning the routes starting from the $3p$ state in $^3He^+$ [(iv) and (v)], $P_T(2)$ is expressed by

$$P_T(2)=0.407+0.296A_0^{\rm col}\ , \tag{19}$$

where $A_0^{\rm col}$ for $L=1$ varies from -1 to $\frac{1}{2}$. Concerning the routes starting from the $3s$ state in $^3He^+$ [(vi) and (vii)], $P_T(3)$ is expressed by

$$P_T(3)=0.407\ . \tag{20}$$

It is noted that P_T is constant for this case because no alignment parameter is present in the case of $L=0$.

P_T is determined only from L of the captured state and is independent of the principal quantum number n. As described in Sec. IV, we cannot experimentally distinguish the above $P_T(i)$'s individually but observe only their averaged value $P_T^{\rm av}$ weighted by their respective cross sections $\sigma(i)$. This is symbolically expressed by

$$P_T^{\rm av}=\frac{\sum_{i=1}^{3}\sigma(i)P_T(i)}{\sum_{i=1}^{3}\sigma(i)}\ . \tag{21}$$

As detailed in Sec. IV, the initial sodium polarization and the final $^3He^+$ polarization were measured, from which the polarization transfer coefficients $P_T^{\rm ob}$ were deduced. For comparison of $P_T^{\rm ob}$ with the theoretical results, the averaged polarization transfer coefficient $P_T^{\rm av}$ were evaluated using Eq. (21). For this purpose, it is necessary to calculate not only alignment parameters but the cross sections. For evaluating the alignment parameter defined by Eq. (14), we calculated each σ_{lnm} individually, where m is the azimuthal quantum number of the orbital angular momentum.

Since the measurement of $P_e(1s)$ is not easy, we performed, in the present work, an indirect method. The capture and photon emission processes were done with a magnetic field strong enough to decouple the hyperfine interactions of the $^3He^+$ ion. The $^3He^+$ ions emerging to the region of zero field nonadiabatically will be nuclear polarized. The degree of the nuclear polarization P_N is approximately expressed in terms of the atomic polarization [17] of the $^3He^+$ ions $P_e(1s)$ as

$$P_N\sim\tfrac{1}{2}P_e(1s)\ , \tag{22}$$

which indicates that one can obtain the degree of the electronic polarization for the $^3He^+$ ions by the measurement of the nuclear polarization. The measurement of the nuclear polarization, on the other hand, can be determined by means of beam-foil spectroscopy as described in Sec. IV.

III. OUTLINE OF SEMICLASSICAL IMPACT-PARAMETER METHOD

In this section, calculations of the cross sections and the alignment parameters of the capture process for the $^3He^{2+}+\vec{Na}$ system, including $^3He^+$ states up to $4f$, are carried out in the framework of the semiclassical impact-parameter method [16,18]. This method is valid for an atom-ion collision at an impact energy larger than a few eV. Internal motions are treated quantum mechanically, while relative motions are treated as classical straight-line trajectories. An atomic (plane-wave) form of the electron translation factor (ETF), in a first-order approximation in collision velocity, is used to account for the electron motion between colliding nuclei.

Calculations of the capture cross sections for the $He^{2+}+Na$ system were attempted by Shingal, Noble, and Bransden, [16] and Kumar, Lane, and Kimura [18]. The latter calculations were for an impact energy range from 0.4–40 keV/amu in the lab using the molecular basis expansion method. The former calculations were over an impact energy range from 2.5–66.7 keV/amu using the atomic basis expansion method. Calculations were consistent with each other over the overlapping range of impact energy, e.g., the difference of the partial cross sections feeding to $n=3$ states between two models was only 8% at an impact energy of 13 keV/amu. In addition, both calculations could reproduce the experimental results within 10% differences.

We thus performed calculations according to a prescription of Kumar, Lane, and Kimura [18]. In order to increase the precision of the calculation, a few improvements were made. Since the basic details of the calculation have been published [18], this section only emphasizes the mentioned improvements.

A. Electronic states

The electronic states have been calculated by using the method of valence-bound configuration interactions including a pseudopotential. For the Na^+ core we used a pseudopotential expressed by

$$V(\mathbf{r})=\sum_l\sum_m V_l(r)|Y_{lm}\rangle\langle Y_{lm}|\ , \tag{23}$$

where $|Y_{lm}\rangle$ are spherical harmonics and $V_l(r)$ is given by

$$V_l(r)=A_le^{-\xi r^2}-\frac{\alpha_d}{2(r^2+d^2)^2}-\frac{\alpha_q}{2(r^2+d^2)^3}-\frac{1}{r}\ . \tag{24}$$

Here, the parameters used in Eq. (24) are from Bardsley [19], the orbital exponents of the basis sets for Na are from Kimura, Olson, and Pascale [20], while those for He^+ are from Sato and Kimura [21]. However, in order to improve the precision of the calculation, a few bases thus created from Slater exponents and summarized in Table I were added. Using these basis sets we calculated the electronic states for Σ, Π, and Δ states with 29, 14, and 6 configurations, respectively. In order to examine the precision of the calculated results, we estimated the ionization potentials of Na and He^+ by using the above

TABLE I. Orbital exponents of the Slater-type orbital basis function.

He^+		Na	
Orbit	Exponent	Orbit	Exponent
1s	2.0	3s	0.79
	1.0	3d	1.484
	0.666 667		0.337
	0.5	4s	2.487
2s	1.0		0.694
	0.666 667		0.372
	0.5	4p	0.721
2p	1.0		0.558
	0.666 667	5s	0.290
	0.5		
3s	0.666 667		
	0.5		
3p	0.666 667		
	0.5		
3d	0.666 667		
	0.5		
4s	0.5		
4p	0.5		
4d	0.5		
4f	0.5		

electronic states. It was found that the deviation of the calculated results from the reliable spectroscopic data [22] was not more than 0.04%, ensuring sufficient precision for calculations of the cross sections and alignment parameters. There is no sizable difference between the adiabatic potential-energy curve thus obtained and those given by Kumar, Lane, and Kimura [18]. We thereafter solve the radial and rotational couplings necessary for collision cross-section calculations.

B. Collision dynamics

We solved a first-order close-coupled linear equation by substituting the scattering wave functions consisting of the product between the electron wave function and the atomic type ETF in the time-dependent Schrödinger equation. Differing from the procedure of Kumar, Lane, and Kimura [18], in which 14 channels consisting of eight Σ states and six Π states were employed, we took into account 18 channels consisting of ten Σ states, six Π states, and two Δ states. Since the energy differences between Σ, Π, and Δ states were inversely proportional to the internuclear distance, it was essential to solve the closed-coupled equation to large distances ($R_{max}=45a_0$, where $a_0=0.529\times10^{-8}$ cm). Moreover, since the square of the scattering amplitude corresponded to the transition probability at a certain impact parameter **b**, the partial cross section σ_{nlm} was calculated by integrating this transition probability times **b** with respect to **b**. However, it is not possible to directly obtain the partial cross section from the solution of the close-coupled equation since the captured electron states of the $^3He^{2+}$+Na system intermix via the Stark effect because of the monoelectron system for $^3He^+$. We calculated, instead, the partial cross section by converting the electronic states to the pure atomic states with *nlm*. This was done by using the coefficients in the electron wave functions. The total cross section and the alignment parameter could thus be obtained from this partial cross section.

IV. EXPERIMENT

The experiment has been performed at the Research Center for Nuclear Physics (RCNP), Osaka University. Most of the initial data were taken with a 2.45-GHz ECR (electron cyclotron resonance) ion source [23]; latter measurements of the $^3He^+$ yield following the capture process were carried out with a new ECR ion source, i.e., Neomafios-10-GHz ion source [24], the setup of which is schematically shown in Fig. 1. The setup is divided into the following four sections: (i) an ECR ion source for production of $^3He^{2+}$ ions, (ii) a sodium cell where the capture process occurs, (iii) a polarimeter for measuring the final-state polarization after cascade photon emissions, and (iv) a pumping laser and a probe laser for polarization monitoring. Since each constituent has already been presented, only a summary emphasizing the recent progress will be described in this section.

A. Production of $^3He^{2+}$ ion and polarized electron capture

A performance test of the 2.45 GHz ECR ion source revealed that a few $e\mu$A $^3He^{2+}$ beams arrived at the Faraday cup after magnetic analysis. With this ECR ion source the maximum polarized $^3He^+$ current following the capture process was only 40–50 $e\mu$A. This is sufficient for the present purpose but insufficient for practical use as a polarized ion source. In order to increase the polarized beam intensity, we replaced this ECR ion source with a more powerful one, i.e., a Neomafios-10-GHz ion source, which was bought from Grenoble, France. The new ECR produces a more than 300-$e\mu$A $^3He^{2+}$ beam, as shown in Fig. 2.

Through focusing elements, the $^3He^{2+}$ beams were introduced to a sodium cell, in which a sodium vapor was polarized by means of laser optical pumping. The laser light frequency was tuned to the $D1$ line of the sodium atom. In order to keep the sodium polarization large against the wall depolarization, an axial magnetic field of 0.3 T was applied to the sodium cell. Though the strength of the applied magnetic field was insufficient to fully decouple the local field generated by a dry-film coated wall of the sodium cell, a considerable amount of the sodium polarization (0.2–0.5) was still present [25]. Another laser light tuned midway between the $D1$ and $D2$ lines was used for monitoring the sodium polarization and the sodium vapor thickness by means of the Faraday rotation method. The rotation angle of the linear polarization was reliably measured to better than 0.1° by introducing a beam splitter cube and photodiodes.

In Fig. 3(a), $^3He^+$ beam currents resulting from the capture process are plotted as a function of the sodium vapor thickness. The $^3He^+$ beam current increased with increasing vapor thickness, but unexpectedly dropped above a critical vapor thickness. This singular behavior

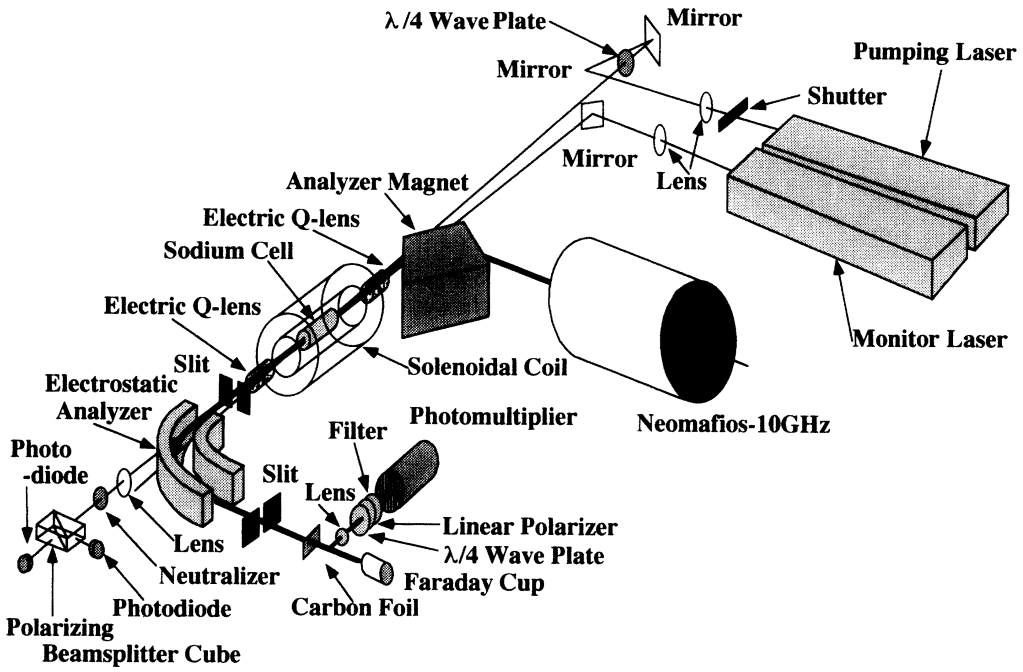

FIG. 1. A schematic view of the instrument used for the measurement of polarization transfer coefficients.

might be a consequence of a sequential double electron-capture process, i.e., with increasing vapor thickness, the probability for the $^3He^+$ ions to capture another electron increases. This will be discussed in more detail in Sec. V. From a practical point of view, this phenomenon determines the upper limit of the polarized beam intensity for the polarized ion source.

In Fig. 3(b), $^3He^+$ beam currents are plotted as a function of the primary $^3He^{2+}$ currents, for which the sodium vapor thickness was kept just below the critical point where the maximum $^3He^+$ beam current was obtained.

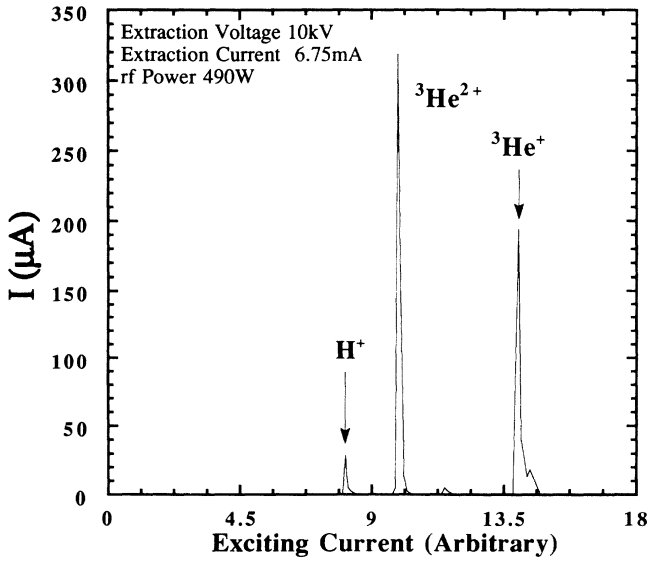

FIG. 2. Charge distribution for ^3He gas ionized by the Neomafios-10-GHz ion source.

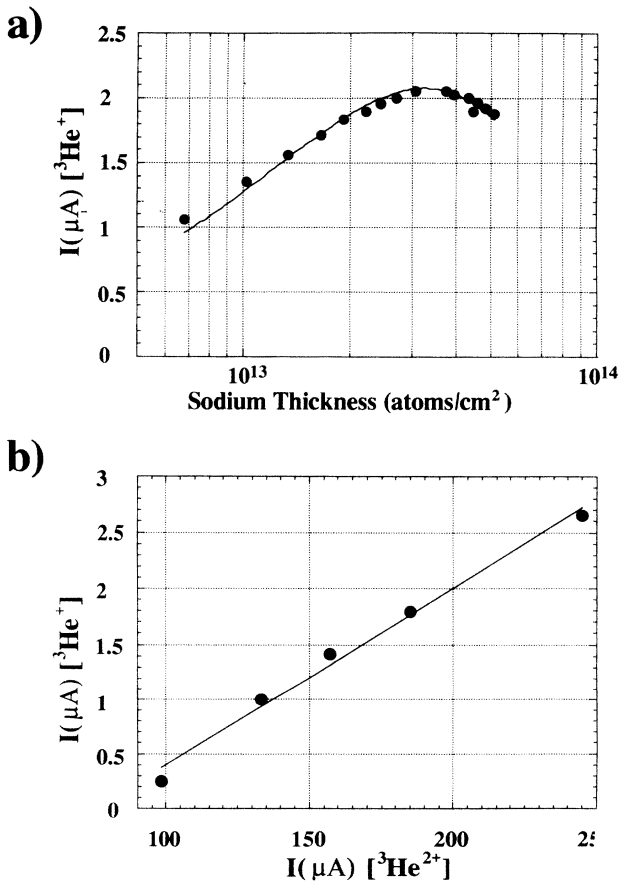

FIG. 3. (a) $^3He^+$ beam current measured as a function of sodium vapor pressure. The solid curve is the best-fitted theoretical curve. (b) $^3He^+$ beam current measured as a function of the primary $^3He^{2+}$ current.

In addition, the maximum $^3He^+$ beam current was larger than 2.6 $e\mu$A. However, this value is still orders of magnitude less than the expected value estimated from the sodium vapor thickness and the capture cross section. This may be improved by employing a better beam transport system.

B. Measurement of polarization transfer coefficient

The final polarization $P_e(1s)$ is determined indirectly by measuring the $^3He^+$ nuclear polarization P_N with beam-foil spectroscopy, the description of which has already been published [8]. Therefore, only an update of recent accomplishments is addressed.

When the $^3He^+$ ion comes out of the sodium cell, in which a 0.3-T magnetic field is applied, a field-free region, a certain amount of the electronic polarization is converted to $^3He^+$ nuclear polarization through the hyperfine interaction. Then, after passing through an electrostatic analyzer, the polarized $^3He^+$ ion is incident upon a thin carbon foil with a thickness of 4 μm without changing the polarization direction. In order to avoid depolarization during beam transport between the capture region and the polarimeter, a holding field of a few gauss is applied axially. The $^3He^+$ ions penetrating the foil are mostly ($\geq 90\%$ at 20 keV impact energy) neutralized but remain in excited states. The surface of the carbon foil is normal to the beam direction, thus avoiding additional electronic polarization due to the tilting foil effect.

The excited ^3He I atoms formed in the carbon foil, then, decay to the ground or metastable states by emitting photons in flight. During in-flight photon emission, the nuclear polarization is periodically transferred to the electron of the neutral atom. As a consequence, a circular polarization is generated for emitted photons. In other words, the amount of nuclear polarization can be determined from the measurement of the circular polarization of emitted photons. The circular polarization is measured by a photon polarimeter composed of a photomultiplier, a wavelength filter, a linear polarizer, and a quarter wavelength plate, as schematically shown in Fig. 1. Among the various photon candidates suitable for measuring the circular polarization, we have chosen a 389-nm line corresponding to the transition between the $3\,^3P_J$ ($J=2,1,0$) and the 2^3S_1 state in ^3He I because its intensity is relatively strong and its lifetime ($\tau \sim 100$ ns) is long enough for application of beam-foil spectroscopy. The calculated result of the time-dependent analyzing power $A(t)$ [8,26] for this transition is given by

$$A(t)=\tfrac{2}{27}(1-\cos\omega_1 t)+\tfrac{2}{15}(1-\cos\omega_2 t)\ , \tag{25}$$

assuming that the 3^3P_J state cascading down from higher excited states in the ^3He I is negligible. Here, ω_1 and ω_2 are the hyperfine angular frequencies between the ($J=1$, $F=\frac{3}{2}$) and ($J=1$, $F=\frac{1}{2}$) and the ($J=2$, $F=\frac{5}{2}$) and ($J=2$, $F=\frac{3}{2}$) states of ^3He I (3^3P_J), respectively. Substituting the appropriate values $\omega_1/2\pi=2.85$ GHz, $\omega_2/2\pi=0.539$ GHz [27] into Eq. (24), the time-dependent analyzing power is represented in terms of the distance z from the carbon target as shown in Fig. 4, where the ^3He beam energy is 6.67 keV/amu. Since the period the quantum beat is less than 5 mm for an impact energy range of 5.33–9.33 keV/amu and the resolution of the polarimeter along the beam trajectory is larger than 5 mm, it is valid to employ the time-averaged analyzing power. The resultant time-averaged value $\overline{A}$ is

$$\overline{A}=0.207\ . \tag{26}$$

The nuclear polarization P_N of the $^3He^+$ ground state is deduced from the asymmetry ε defined by

$$\begin{aligned}\varepsilon&=\frac{N_{\rm on}}{N_{\rm off}}-1\ ,\\ &=\overline{A}P_N\ ,\end{aligned} \tag{27}$$

where $N_{\rm on}$ and $N_{\rm off}$ are the counting numbers with pumping laser on and off, respectively. P_N is then converted to the electronic polarization $P_e(1s)$ of the $^3He^+$ ground state by using Eq. (22).

Figure 5 exemplifies the observed asymmetries ε plotted against the sodium polarization $P_{\rm Na}$ taken at the $^3He^{2+}$ impact energy of 6.67 keV/amu. To ensure that

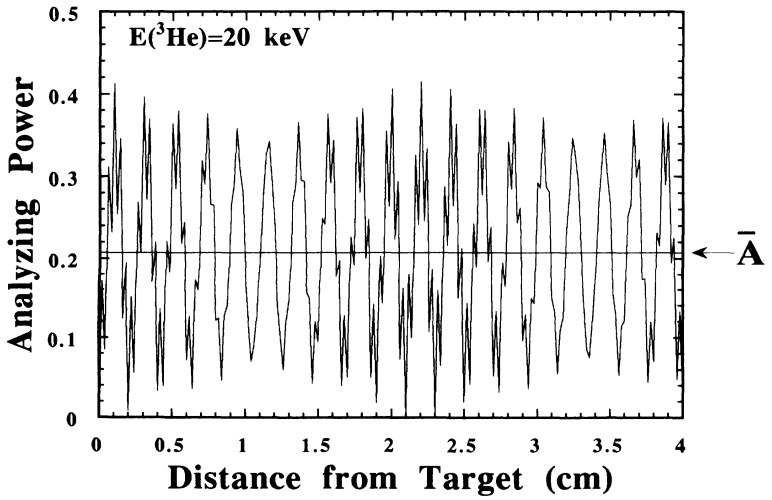

FIG. 4. Calculated analyzing power for the circularly polarized photons corresponding to the transition between the $3\,^3P_J$ ($J=2$, 1, and 0) and $2\,^3S_1$ state in ^3He I plotted as a function of the position starting from the carbon target, where ^3He I energy is 6.67 keV/amu. The horizontal line indicated by $\overline{A}$ is a time-averaged analyzing power.

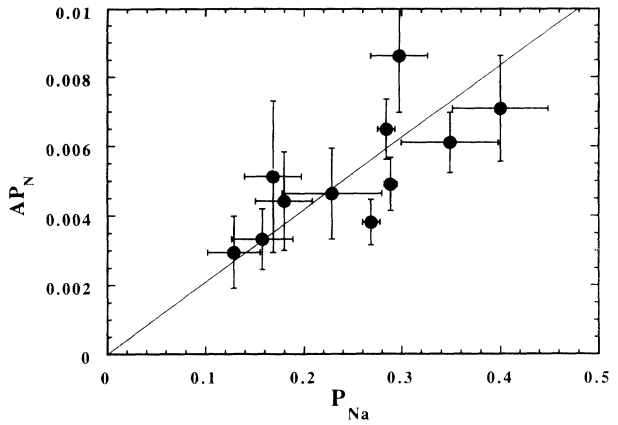

FIG. 5. The observed asymmetries ε plotted as a function of the sodium polarization measured at the $^3He^{2+}$ impact energy of 6.67 keV/amu.

the observed asymmetries were not due to the atomic effect caused by the tilting foil effect but to the nuclear effect, beam-foil spectroscopy was carried out for the $^4He^+$ ion, which has no nuclear polarization because $I=0$, that was populated by the polarized electron-capture process. The result obviously showed no evidence for asymmetry, from which the observed asymmetries for $^3He^+$ are really due to the nuclear effect.

From this result, one can deduce the observed polarization transfer coefficient P_T^{ob} defined by

$$P_T^{ob}=\frac{P_e(1s)}{P_{Na}} . \tag{28}$$

The measurement of P_T^{ob} at impact energies other than 6.67 keV/amu is not straightforward because the analyzing power $\bar{A}$ defined by Eq. (25) might be dependent on impact energy. The energy dependence of $\bar{A}$ may be explained by speculating that the ratio of the direct population of the 3^3P_J state to the indirect feeding from the higher excited states through cascade photon emissions could vary according to the change of impact energy. In order to examine the impact energy dependence of $\bar{A}$, the carbon target is insulated so that a high voltage could be applied to the target. The asymmetry ε is observed by applying a high voltage V (keV) to the target with the impact energy kept at 6.67 keV/amu, which enables us to measure the change of the asymmetry, i.e., the change of $\bar{A}$ in an impact energy range of (6.67−V/3.016) keV/amu. In the present measurement, V is varied from −8 to 8 kV. The variation of the asymmetry with respect to the value obtained at $V=0$, if it exists, should be due to the impact energy dependence of $\bar{A}$. No sizable energy dependence for $\bar{A}$ is observed, although the errors are too large to decisively rule it out. After checking this point, we observe P_T^{ob} at other impact energies without the target potential. The results assuming constant $\bar{A}$ are indicated by the open triangles in Fig. 6.

As a more reliable method to test the impact energy dependence of $\bar{A}$, we apply a high voltage V to the carbon target such that the change in impact energy may be compensated as it deviates from 6.67 keV/amu. Thus, the impact energy incident on the carbon target can be effectively maintained at 6.67 keV/amu. The closed circles in Fig. 6 are P_T^{ob} deduced by this method, with the error bars representing the standard deviation of repetitive measurements.

V. RESULTS AND DISCUSSION

The observed P_T^{ob}'s (Fig. 6) were analyzed by the semiclassical impact-parameter method, which was described in Sec. III. In order to examine the validity of the present theoretical calculation, we compared the calculated capture cross sections with the observed values for the ^4He+Na system [1,28]. In Fig. 7, the capture cross sections of the $^3He^{2+}+Na$ system scaled from observation for the $^4He^{2+}+Na$ system are plotted along with the calculated results. Data indicated by the closed circle are total capture cross sections from Ref. [1]. Data indicat-

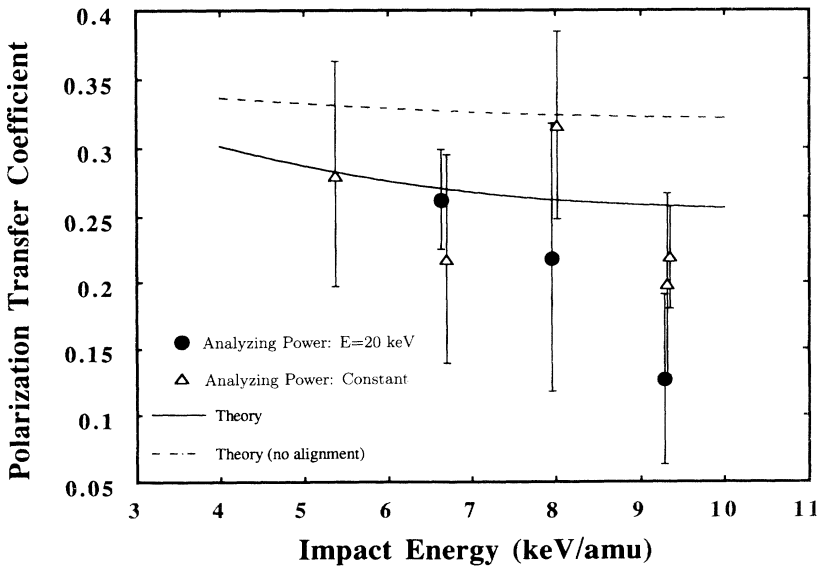

FIG. 6. Impact energy dependence of the averaged polarization transfer coefficients. The closed circles are the experimental results, in which $\bar{A}$ is properly corrected by the standard value at 6.67 keV/amu. The open triangles are the experimental results extracted assuming a constancy of $\bar{A}$. The dashed curve is the theoretical result with $A_0^{col}=0$. The solid curve is the full theoretical result involving the alignment parameters for 3*d*, 3*p*, and 3*s* states in $^3He^+$.

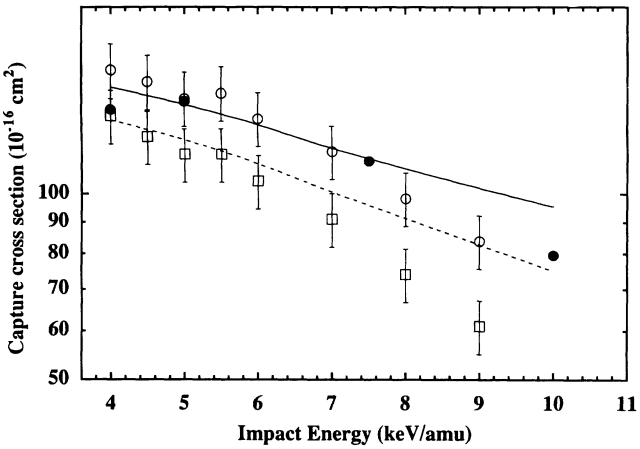

FIG. 7. Capture cross sections for the $^3He^{2+}+Na$ system scaled from the observed values for the $^4He^{2+}+Na \rightarrow {}^4He^+ + Na^+$ system are compared with the calculated results. Data indicated by the closed circles are observed total capture cross sections referred from Ref. [1]. Data indicated by the open circles are observed partial cross sections feeding to $n=3$ and 4 states in $^3He^+$ and are referred from Ref. [28]. Data indicated by the open squares are the observed partial capture cross section feeding to $n=3$ states in $^3He^+$. The solid curve is the theoretical result including all the capture cross sections up to $n=4$ states in $^3He^+$. The dotted curve is the theoretical capture cross sections feeding to $n=3$ states in $^3He^+$.

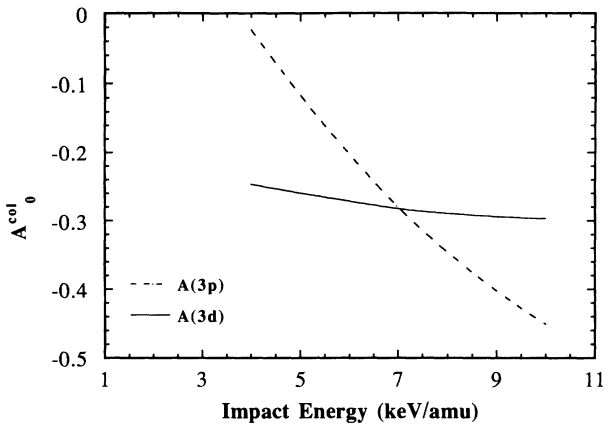

FIG. 8. The calculated alignment parameters for the $3d$ and $3p$ states in $^3He^+$ populated immediately after the captured process.

ed by the open and closed circles are, respectively, partial capture cross sections feeding to the $^3He^+$ states with $n=3,4$ and $n=3$ states, which were obtained by observing decaying photons [28]. The solid curve is the theoretical capture cross sections summed over states with $n=1-n=4$. The dotted curve is the theoretical capture cross sections for the states with $n=3$. Figure 7 shows that main capture cross sections are due to the capture of the $n=3$ states in $^3He^+$. In the impact energy region lower than 7 keV/amu, the theoretical results reproduce not only the observed energy dependence but also the absolute values for both total and partial capture cross sections. In the higher impact energy region, on the other hand, the theoretical results seem to be, somehow, larger than the experimental ones. However, the calculation, as a whole, reproduces the experimental results, which confirms the appropriateness of this approach in the impact energy region of interest.

Encouraged by this finding, calculations of the P_T^{av}'s were attempted. As already mentioned, P_T^{av}'s were evaluated from Eq. (21) as the weighted sum of the three main captured states in $^3He^+$, i.e., $3d$, $3p$, and $3s$. Each P_T is expressed in terms of the alignment parameter as seen in Eqs. (18)–(20). The alignment parameters evaluated by calculating associated partial capture cross sections σ_{nlm} are shown in Fig. 8 for the captures to the $3d$ and $3p$ states. (Note that no alignment exists for the capture to the $3s$ state.) The A_0^{col}'s, as a whole, deviate in the negative direction for both states, i.e., the magnetic substate with $m=0$ is preferably populated. In other words, the angular-momentum transfer tends to be perpendicular to the beam axis. In addition, A_0^{col}'s decrease for both states as the impact energy is increased. These behaviors are intuitively understood; in a low-impact-energy region the angular-momentum transfer favors the beam direction because formation of atomic orbits becomes influential relative to an angular-momentum transfer due to an orbital motion of the projectile trajectory. In the high-energy region, the formation of atomic orbits becomes less important. Finally, of particular interest is the different impact energy dependent of A_0^{col} for the $3d$ and $3p$ states, i.e., A_0^{col} of the $3p$ state changes more drastically than that of the $3d$ state.

Substituting the calculated results of A_0^{col}'s in Eq. (18)–(21), the polarization transfer coefficients P_T^{av}'s are evaluated. The calculated results are plotted as solid and dashed curves in Fig. 6, where the dashed curve is the result obtained with A_0^{col} switched off, i.e., $A_0^{col}=0$, while the solid curve is the full calculation. As shown in this figure, the observed P_T^{ob}'s seem to favor the solid curve rather than the dashed one, suggesting the presence of the alignment parameter. In addition, the gentle decrease of P_T^{ob} with increasing impact energy is reproduced by the theoretical calculations.

The P_T discussed above just corresponds to an upper limit for the ^3He nuclear polarization as long as the full sodium polarization is realized. The polarized electron-capture process at lower impact energies is more advantageous for obtaining larger ^3He nuclear polarization, because P_T increases with decreasing impact energy.

So far, no theoretical analyses of P_T^{av} using the semiclassical impact-parameter method have been attempted. The calculation of P_T^{av} for the capture processes of multicharged heavy ions incident on polarized alkaline atoms is of particular relevance in planning for the polarized heavy-ion source. It seems beneficial to estimate upper limits on nuclear polarizations for ions resulting from the cascade photon emissions after electron-capture processes. We calculated them [29] for the incidence of fully stripped heavy ions on the sodium atom forming hydrogenlike atoms assuming the simple cascade photon decay model with no alignment parameter. We assume that the capture process dominates for the states with electron

binding energy approximately equal to that of the sodium $3s$ state.

From this constraint, the principal quantum number n of the captured state might be assigned. Regarding the l value of the captured state, we take the maximum possible value, i.e., $l=n-1$, thus allowing severe constraints on evaluation of the nuclear polarization. In Table II, we summarize the calculated values for the nuclear polarizations thus obtained for light heavy ions when the initial sodium polarization is 1.0. Here, the calculated nuclear polarizations are based on the Sona transition method, assuming an efficient conversion of electron to nuclear polarization [30]. The last column in Table II shows the calculated values of the decoupling fields necessary to decouple the hyperfine interaction by using Eq. (1). This table is indicative of the presence of sizable nuclear polarizations P_N irrespective of ion species, though the amount of the nuclear polarization seems to decrease with increasing mass number. This is encouraging if one wishes to generalize this approach to polarized heavy-ion sources. However, further theoretical calculations are needed to precisely predict nuclear polarizations.

All discussion so far have been concerned with capture processes accompanying a single electron. However, we found indirect evidence for the double electron capture, as pointed out in Sec. IV. The intensity drop of $^3He^+$ with increasing sodium thickness in Fig. 3(a) is caused by the $^3He^+$ beam loss resulting from the formation of ^3He atoms due to an additional electron capture of $^3He^+$ ions. In the appendix, the $^3He^+$ beam intensity is calculated, allowing for the sequential double electron capture. According to the result of the Appendix, the number ratio of $^3He^+$ ions n_1 to the primary $^3He^{2+}$ ions $n_2(0)$ is obtained as shown by

$$\frac{n_1}{n_2(0)}=\frac{\sigma_{21}}{\sigma_{10}-\sigma_{21}}(e^{-\sigma_{21}L}-e^{-\sigma_{10}L}) , \tag{29}$$

where L is sodium target thickness in unit of atoms/cm^2 and σ_{10} and σ_{21} are the cross sections for the capture processes denoted by $^3He^+\rightarrow{}^3He$ and $^3He^{2+}\rightarrow{}^3He^+$, respectively. In deducing the above formula the effect of the direct double capture process [31] was neglected because the measured cross section for it was less than σ_1 or σ_2 by about $\frac{1}{50}$ [1]. We fit the experimental result in Fig. 3(a) with Eq. (28) by means of the least-squares-fitting method. The best-fitted curve is shown by the solid curve in Fig. 3(a) and the deduced values for σ_{10} and σ_{21} are given by

$$\sigma_{10}=3.10\times10^{-14}\ \text{cm}^2 , \tag{30}$$

$$\sigma_{21}=3.07\times10^{-14}\ \text{cm}^2 . \tag{31}$$

Though these values are larger than the direct observation [1,28] by about 2–3 times, the observed behavior in Fig. 3(a) is well reproduced by the present calculation. The discrepancy of the capture cross sections between the present result and the direct observation suggests the presence of other effects that have not been addressed, e.g., multiple scattering of $^3He^{2+}$ and $^3He^+$ ions traveling in sodium vapor, the apparent increase of the sequential capture cross section as a result of sodium excitation, and so on.

It is uncertain whether or not such a sequential capture process affects the polarization. In order to clear up this point, the polarization measurement by changing the sodium vapor thickness is required.

TABLE II. Expected nuclear polarization populated through the capture of the spin-polarized electron and subsequent photon decay assuming the simple cascade photon decay model with no alignment parameter. n and l are the principal and orbital quantum numbers for the captured electron, respectively. P_T is the calculated polarization transfer coefficient. P_N is the expected final nuclear polarization by using the Sona transition method.

Nucleus	Nuclear spin	n	l	P_T	P_N	B_{hf} (T)
$^6Li^{2+}$	1	5	4	0.234	0.156	0.2
$^7Li^{2+}$	$\frac{3}{2}$	5	4	0.234	0.118	0.53
$^9Be^{3+}$	$\frac{3}{2}$	6	5	0.219	0.110	0.46
$^{10}B^{4+}$	3	8	7	0.202	0.058	0.68
$^{11}B^{4+}$	$\frac{3}{2}$	8	7	0.202	0.102	2.03
$^{13}C^{5+}$	$\frac{1}{2}$	10	9	0.192	0.192	2.76
$^{14}N^{6+}$	1	11	10	0.188	0.126	1.26
$^{15}N^{6+}$	$\frac{1}{2}$	11	10	0.188	0.188	1.76
$^{17}O^{7+}$	$\frac{5}{2}$	13	12	0.183	0.006	3.52

VI. CONCLUSIONS

We have investigated experimentally and theoretically the polarized electron-capture process of the $^3He^{2+}+Na$ system. The polarization transfer coefficient P_T defined by the ratio of the final electronic polarization of the $^3He^+$ ion to the initial alkaline polarization was obtained in an impact energy range of 5.33–9.33 keV/amu. This system provides an important test case for investigation of the capture process since the main interaction can be described in a quasi-one-electron model. This system can be reliably modeled with the advanced semiclassical impact-parameter method. The theoretical calculations predicted both the absolute values and the impact energy dependence of the experimental capture cross sections. The theoretical results were compared with the observed polarization transfer coefficients. It was found that the experimental polarization transfer coefficients were reasonably reproduced by the theoretical calculations, allowing the presence of the alignment parameters for each captured state including $3d$, $3p$, and $3s$ in $^3He^+$.

The theoretical approach using the semiclassical impact-parameter method successfully reproduced not only the capture cross sections but also the polarization transfer coefficients, which are even more sensitive to the details of the subtle theoretical treatment. The present success suggests that the semiclassical impact-parameter method will provide a good description of the capture processes for systems like $^3He^{2+}+\vec{Na}$, in which only one electron plays a major role.

ACKNOWLEDGMENTS

The authors would like to express their sincere gratitude to Professor Tawara for pointing out the physical importance of polarization phenomena in an atom-ion collision process. They are also indebted to Professor Nakamura, Professor Kimura, Professor Mori, Professor Anderson, Professor Nusharov, Professor Steffens, and Professor Fick for their encouragement throughout this work, and to Dr. Tamura for his illuminating contribution in the calculation of the cascade photon decay model. Thanks are also due to Professor Geller, Dr. Melin, and Dr. Ludwig, for successful fabrication, installation, and operation of the Neomafios-10-GHz ion source. The authors acknowledge Professor Itahashi and the cyclotron crew of the RCNP for their patient support. They are also grateful to Professor Greenfield for his critical reading of this manuscript. A part of this work was financially supported by a grant-in-aid from the Ministry of Education, Japan.

APPENDIX: ESTIMATION OF $^3He^+$ YIELD

We calculate the $^3He^+$ yield resulting from electron capture of $^3He^{2+}$ ions incident on the sodium vapor target allowing double electron capture forming neutral ^3He atoms by a sequential process. The effect of the direct double electron capture is neglected because its cross section is far less than single-electron-capture cross sections. As shown in Fig. 9, we define the numbers of $^3He^{2+}$ and $^3He^+$ ions at a target thickness x by $n_2(x)$ and $n_1(x)$, respectively. Changes of these numbers due an additional target thickness Δx are given by

$$\Delta n_2(x) = -\Delta x \sigma_{21} n_2(x) , \tag{A1}$$

$$\Delta n_1(x) = -\Delta x \sigma_{10} n_1(x) + \Delta x \sigma_{21} n_2(x) , \tag{A2}$$

where σ_{21} and σ_{10} are the capture cross sections for $^3He^{2+}$ and $^3He^+$ ions to form $^3He^+$ and ^3He ions, respectively. From Eqs. (A1) and (A2), we obtain a set of simultaneous equations expressed by

$$\frac{dn_2}{dx} = -\sigma_{21} n_2 , \tag{A3}$$

$$\frac{dn_1}{dx} = -\sigma_{10} n_1 + \sigma_{21} n_2 . \tag{A4}$$

The solution of Eq. (A3) is

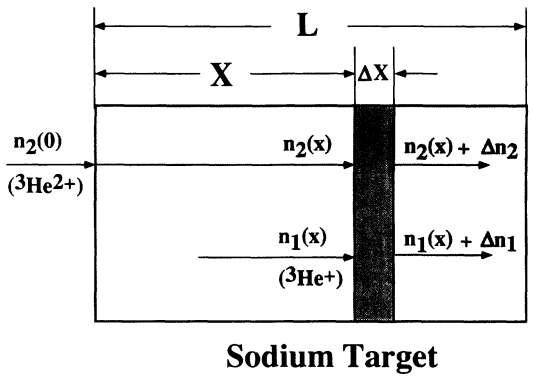

FIG. 9. A schematic view showing a sequential double electron capture process.

$$n_2(x) = n_2(0) e^{-\sigma_{21} x} , \tag{A5}$$

where $n_2(0)$ is the number of incident $^3He^{2+}$ ions at $x=0$. Substituting Eq. (A5) in Eq. (A4), we obtain a linear differential equation for n_1 as expressed by

$$\frac{dn_1}{dx} + \sigma_{10} n_1 = \sigma_{20} n_2(0) e^{-\sigma_{20} x} . \tag{A6}$$

This equation is analytically solved and given by

$$n_1 = \frac{\sigma_{21}}{\sigma_{10} - \sigma_{21}} n_2(0) e^{-\sigma_{21} x} + C e^{-\sigma_{10} x} , \tag{A7}$$

where C is a constant to be determined from the initial condition that $n_1(x)$ is zero at $x=0$. C thus obtained is given by

$$C = -\frac{\sigma_{21}}{\sigma_{10} - \sigma_{21}} n_2(0) . \tag{A8}$$

Substituting Eq. (A8) in Eq. (A7), the number of $^3He^+$ ions is given by

$$n_1(x) = \frac{\sigma_{21}}{\sigma_{10} - \sigma_{21}} n_2(0) (e^{-\sigma_{21} x} - e^{-\sigma_{10} x}) . \tag{A9}$$

In consequence, the number ratio of $^3He^+$ ions to the primary $^3He^{2+}$ ions is expressed in terms of the sodium vapor thickness L (atoms/cm^2) as

$$\frac{n_1}{n_2(0)} = \frac{\sigma_{21}}{\sigma_{10} - \sigma_{21}} (e^{-\sigma_{21} L} - e^{-\sigma_{10} L}) . \tag{A10}$$

[1] R. D. DuBois and L. H. Toburen, Phys. Rev. A **31**, 3603 (1985).

[2] A. V. Vinogradov and I. I. Sobelman, Zh. Eksp. Teor. Fiz. **63**, 2113 (1972) [Sov. Phys. JETP **36**, 1115 (1973)].

[3] W. Jitschin, A. Kaschuba, H. Kleinpoppen, and H. O. Lutz, Z. Phys. A **304**, 69 (1982).

[4] R. Hippler, M. Faust, R. Wolf, H. Kleinpoppen, and H. O. Lutz, Phys. Rev. A **36**, 4644 (1987).

[5] W. Haeberli, in *Proceedings of the Second International Symposium on Polarization Phenomena in Nuclear Physics, Karlsruhe, West Germany,* edited by P. Huber and H. Schopper (Berkhauser, Stuttgart, 1966), p. 643.

[6] L. W. Anderson, Nucl. Instrum. Methods **167**, 363 (1979).

[7] Y. Mori, A. Takagi, K. Ikegami, S. Fukumoto, and A. Ueno, J. Phys. Soc. Jpn. **55**, 453 (1986).

[8] T. Ohshima, K. Abe, K. Katori, M. Fujiwara, T. Itahashi, H. Ogata, M. Kondo, and M. Tanaka, Phys. Lett. B **274**, 163 (1992).

[9] C.-J. Liu, N. B. Mansour, Y. Azuma, H. G. Berry, D. A. Church, and R. W. Dunford, Phys. Rev. Lett. **64**, 1354

(1990).
[10] T. Ohshima, M. Tanaka, K. Katori, M. Fujiwara, H. Ogata, M. Kondo, and N. Shimakura, Hyperfine Interact. (to be published).
[11] W. Jitschin, S. Osmitsch, D. W. Mueller, H. Reihl, R. J. Allan, O. Schröder, and H. O. Lutz, Phys. Rev. B **19**, 2299 (1986).
[12] C. D. P. Levy, K. Jayamannna, M. McDonald, R. Ruegg, and P. W. Schmor, in *Proceedings of the Thirteenth International Conference on Cyclotrons and Their Applications, 1992,* edited by G. Dutto and M. K. Craddock (World Scientific, Singapore, 1992), p. 322.
[13] B. H. Bransden and C. J. Joachain, *Physics of Atoms and Molecules* (Wiley, New York, 1990).
[14] C. Liu and R. W. Dunford, J. Phys. B **24**, 2059 (1991).
[15] U. Fano and J. H. Macek, Rev. Mod. Phys. **45**, 553 (1973).
[16] R. Shingal, C. Noble, and B. H. Bransden, J. Phys. B **19**, 793 (1987).
[17] G. G. Ohlsen, J. L. McKibben, R. R. Stevens, Jr., and G. P. Lawrence, Nucl. Instrum. Methods **73**, 45 (1969).
[18] A. Kumar, N. F. Lane, and M. Kimura, Phys. Rev. A **42**, 3861 (1990).
[19] J. N. Bardsley, Case Stud. At. Phys. **4**, 299 (1974).
[20] M. Kimura, R. E. Olson, and J. Pascale, Phys. Rev. A **26**, 3113 (1982).
[21] H. Sato and M. Kimura, Phys. Lett. A **96**, 286 (1983).
[22] S. Bashkin and J. R. Stoner, *Atomic Energy Levels and Grotorian Diagrams IV* (North-Holland, Amsterdam, 1975).
[23] M. Tanaka, T. Ohshima, K. Abe, K. Katori, M. Fujiwara, T. Itahashi, H. Ogata, and M. Kondo, Nucl. Instrum. Methods Phys. Res. Sect. A **302**, 460 (1991).
[24] R. Geller, Ann. Rev. Nucl. Part. Sci. **40**, 15 (1991).
[25] M. Tanaka, T. Ohshima, K. Katori, M. Fujiwara, T. Itahashi, H. Ogata, and M. Kondo, Phys. Rev. A **41**, 1496 (1990).
[26] H. J. Andrä, H. J. Pöhn, A. Gaupp, and R. Fröhing, Z. Phys. A **281**, 15 (1977).
[27] K. Tillmann, H. J. Andrä, and W. Wittmann, Phys. Rev. Lett. **29**, 155 (1973).
[28] A. R. Schlatmann, R. Hoekstra, H. O. Folkerts, and R. Morgenstern, J. Phys. B **25**, 3155 (1992).
[29] T. Ohshima, Ph.D. thesis, Osaka University, 1992 (unpublished).
[30] P. G. Sona, Energ. Nucl. (Paris) **14**, 295 (1967).
[31] A. Nihaus, J. Phys. B **19**, 2925 (1986).

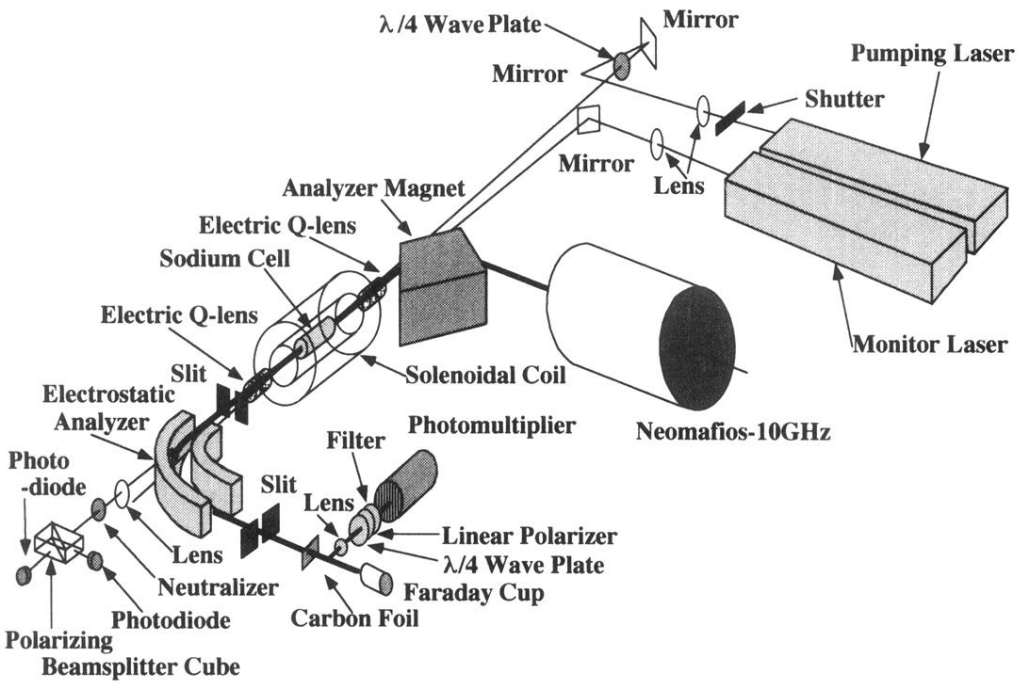

FIG. 1. A schematic view of the instrument used for the measurement of polarization transfer coefficients.

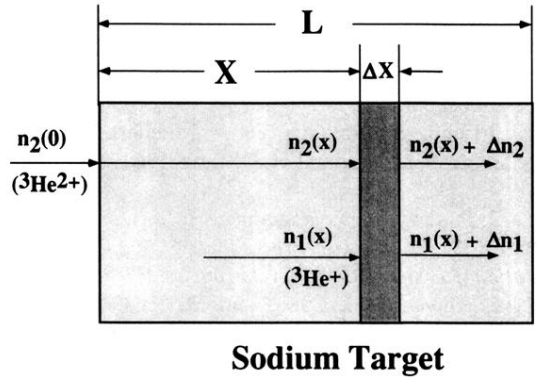

FIG. 9. A schematic view showing a sequential double electron capture process.